

Reweighted sparse deconvolution for high angular resolution diffusion MRI

Alessandro Daducci^{a,*}, Dimitri Van De Ville^{b,d}, Jean-Philippe Thiran^{a,c}, Yves Wiaux^{a,b,d}

^aSignal Processing Lab (LTS5), EPFL, Switzerland

^bMedical Image Processing Lab, EPFL, Switzerland

^cUniversity of Lausanne, Switzerland

^dUniversity of Geneva, Switzerland

Abstract

Diffusion MRI is a well established imaging modality providing a powerful and innovative way to non-invasively probe the structure of the white matter. Despite the potential of the technique, the intrinsic long scan times of these sequences have hampered their use in clinical practice. For this reason, a wide variety of methods have been proposed recently with the aim to shorten acquisition times. Among them, spherical deconvolution approaches have gained a lot of interest for their ability to reliably recover the intra-voxel fiber configuration with a relatively small number of data samples. To overcome the intrinsic instabilities in solving the deconvolution problem, these methods make use of regularization schemes generally based on the assumption that the fiber orientation distribution (FOD) to be recovered is sparse, either explicitly or implicitly. In particular, convex optimization methods have recently been advocated in a compressed sensing perspective for FOD reconstruction from accelerated acquisitions. In this paper, we propose to exploit further the versatility of this powerful framework with the aim to exploit sparsity more optimally. We define a new convex minimization problem for FOD reconstruction through a constrained formulation between sparsity prior and data, also making use of a reweighting scheme. The method has been tested on both synthetic and real data. Experimental results indicate that this approach provides more robust and accurate estimates than the state of the art in terms of both the number and orientation of fiber compartments in each voxel.

Keywords: diffusion MRI, HARDI, reconstruction, spherical deconvolution, compressed sensing

*Corresponding author

Email address: alessandro.daducci@epfl.ch (Alessandro Daducci)

1. Introduction

Fiber-tracking is probably one of the most fascinating applications in diffusion MRI, gathering a lot of attention since the beginning for its ability to reconstruct from the acquired data the main neuronal bundles of the brain. In fact, the diffusion of the molecules in the white matter can be exploited for mapping the brain connectivity, and structures otherwise invisible with other imaging modalities can be highlighted. The study of this structural connectivity is of major importance in a fundamental neuroscience perspective, for developing our understanding of the brain, but also in a clinical perspective, with particular applications for the study of a wide range of neurological disorders.

The most powerful acquisition modality is diffusion spectrum imaging (DSI) (Wedeen et al., 2005). It relies on cartesian signal sampling and is known to provide good imaging quality, but it is too time-consuming to be of real interest in a clinical perspective. Diffusion tensor imaging (DTI) (Basser et al., 1994) is always preferred instead. DTI is a very fast model-based technique providing valuable diagnostic information but, on the contrary, it is unable to model multiple fiber populations in a voxel. In a global connectivity analysis perspective, this constitutes a key limiting factor. Accelerated acquisitions relying on a smaller number of samples while providing accurate estimations of the intra-voxel fiber configuration thus represent an important challenge.

Recently, an increasing number of high angular resolution diffusion imaging (HARDI) approaches have been proposed for tackling this problem. In particular, spherical deconvolution (SD) based methods formed a very active area in this field (Tournier et al., 2004; Alexander, 2005; Tournier et al., 2007; Dell’acqua et al., 2007). These methods rely on the assumption that the signal attenuation acquired with diffusion MRI can be expressed as the convolution of a given response function with the fiber orientation distribution (FOD). The FOD is a real-valued function on the unit sphere (S^2) giving the orientation and the volume fraction of the fiber populations present in a voxel. The response function, or kernel, describes the MRI signal attenuation generated by an isolated single fiber population; it can be estimated from the data or represented by means of parametric functions.

SD approaches represented a big step in reducing the acquisition time of diffusion MRI, but are known to suffer heavily from noise and intrinsic instabilities in solving the deconvolution problem. For this reason, a regularization scheme is normally employed. A variety of approaches have been proposed, which are generally based on the two assumptions that the FOD is (i) a non-negative function and (ii) sparse, i.e. with only a few nonzero values. In fact, at the imaging resolution available nowadays, diffusion MRI is sensitive only to the major fiber bundles and it is commonly accepted that it can reliably disentangle up to 2-3 different fiber populations inside a voxel (Jeurissen et al., 2010). Hence, the FOD can be considered sparse in nature.

The recent advent of *compressed sensing* (CS) theory (Donoho, 2006; Candès et al., 2006; Baraniuk, 2007) provided a mathematical framework for the reconstruction of sparse signal from under-sampled measurements mainly in the

context of convex optimization. CS has inspired new advanced approaches in the last few years for solving the reconstruction problem in diffusion MRI and allowed a further dramatic reduction in the number of samples needed to accurately infer the fiber structure in each voxel. For instance, [Tristán-Vega and Westin \(2011\)](#) and [Michailovich et al. \(2011\)](#) recovered the orientation distribution function (ODF) by using different representations for the response function, while [Merlet et al. \(2011\)](#) and [Rathi et al. \(2011\)](#) focused on the full ensemble average propagator (EAP) of the diffusion process. In this work, however, we focus on spherical deconvolution based methods and the quantity of interest is the FOD. In general, these methods are based on ℓ_1 minimization schemes and the common goal is to recover the FOD with fewest non-zeros that is compatible with the acquired MRI data ([Ramirez-Manzanares et al., 2007](#); [Pu et al., 2011](#); [Landman et al., 2012](#); [Mani et al., 2012](#)). However, we believe that the ℓ_1 norm, identifying the sum of the values of a function, is not adequate for characterizing the actual sparsity lying in the FOD, as the sum of the volume fractions of the compartments inside a voxel is intrinsically equal to 1. Strictly speaking, the FOD sparsity is the number of fiber populations, thus identified by the ℓ_0 norm of the FOD. ℓ_0 norm problems are generally intractable as they are non convex, which explains the usual convex ℓ_1 norm relaxation in the context of compressed sensing. However, among other approaches, a *reweighted ℓ_1 minimization* scheme was developed in order to approach ℓ_0 minimization by a sequence of convex weighted ℓ_1 problems ([Candès et al., 2008](#)).

In this paper, we propose to exploit the versatility of compressed sensing and convex optimization to exploit sparsity more optimally than the state of the art and improve the quality of reconstructions in diffusion MRI. To this aim, we define a new convex minimization problem through a constrained formulation between sparsity prior and data, also making use of a reweighting scheme. We evaluate the effectiveness of our proposal for improving the FOD reconstructions by comparing with existing state-of-the-art spherical deconvolution methods. We report results on both synthetic and real data.

2. Materials and methods

2.1. Intra-voxel structure recovery via spherical deconvolution

As shown by [Jian and Vemuri \(2007\)](#), spherical deconvolution methods can be cast into the following computational framework:

$$S(b, \hat{\mathbf{q}})/S_0 = \int R_{\hat{\mathbf{q}}}(\hat{\mathbf{p}}) f(\hat{\mathbf{p}}) d\Omega(\hat{\mathbf{p}}), \quad (1)$$

where f is the FOD to be estimated, $R_{\hat{\mathbf{q}}}$ represents the response function rotated in direction $\hat{\mathbf{q}} \in S^2$ and the integration is performed over the unit sphere with $\hat{\mathbf{p}} = (\phi, \theta) \in S^2$ and $d\Omega = \sin \phi d\phi d\theta$. $S(b, \hat{\mathbf{q}})$ represents the MRI signal measured on the q-space shell acquired with b-value b in direction $\hat{\mathbf{q}} \in S^2$, while S_0 is the signal acquired without diffusion weighting. The measurement process

can thus be expressed in terms of the general formulation:

$$\mathbf{y} = \Phi \mathbf{x} + \eta, \quad (2)$$

where $\mathbf{x} \in \mathbb{R}_+^n$ is the FOD, $\mathbf{y} \in \mathbb{R}^m$ is measurement vector, $\Phi \in \mathbb{R}^{m \times n}$ is the observation matrix and η represents the acquisition noise.

In the original formulation of [Tournier et al. \(2004\)](#), the FOD \mathbf{x} and the measurements \mathbf{y} were expressed by means of spherical harmonics (SH), and the deconvolution problem was solved by a simple matrix inversion. To reduce noise artifacts, a low-pass filter was applied for attenuating the high harmonic frequencies. The method was improved in ([Tournier et al., 2007](#)) by reformulating the problem as an iterative procedure where, at each iteration, the current solution $\mathbf{x}^{(t)}$ is used to drive to zero the negative amplitudes of the FOD at the next iteration with a Tikhonov regularization ([Tikhonov and Arsenin, 1977](#)):

$$\mathbf{x}^{(t+1)} = \underset{\mathbf{x}}{\operatorname{argmin}} \|\Phi \mathbf{x} - \mathbf{y}\|_2^2 + \lambda^2 \|L^{(t)} \mathbf{x}\|_2^2, \quad (3)$$

where the free parameter λ controls the degree of regularization and $L^{(t)}$ can be understood as a simple binary mask preserving only the directions of small, probably spurious, values of $x^{(t)}$. The ℓ_2 norm regularization term therefore tends to send these values to zero, hence only preserving large values. Interestingly, beyond sending negative values to zero, the operator L thus implicitly promotes a weak version of sparsity. $\|\cdot\|_p$ are the usual ℓ_p norms in \mathbb{R}^n . However, the use of the ℓ_2 norm to model the sparsity prior does not fully guarantee either positivity or sparsity in the recovered FOD. In ([Alexander, 2005](#)) a maximum-entropy regularization was proposed to recover the FOD as the function that exhibits the minimum information content. The method showed higher robustness to noise than previous approaches, but was limited by the very high computational cost and did not promote sparsity. Other regularization schemes have been proposed in the literature, but FOD sparsity has never been addressed with a rigorous mathematical formulation.

Compressed sensing provides a powerful mathematical framework for the reconstruction of sparse signals from a low number of data ([Donoho, 2006](#); [Candès et al., 2006](#)), mainly in the context of convex optimization. According to this theory, it is possible to recover a signal from less samples than the number required by the Nyquist sampling theorem, provided that the signal is sparse in some *sparsity basis* Ψ . Let $\mathbf{x} \in \mathbb{R}^n$ be the signal to be recovered from the $m \ll n$ linear measurements $\mathbf{y} = \Phi \mathbf{x} \in \mathbb{R}^m$ and $\boldsymbol{\alpha} \in \mathbb{R}^n$ a sparse representation of \mathbf{x} through $\Psi \in \mathbb{R}^{n \times n}$. If the observations \mathbf{y} are corrupted by noise and Φ obeys some randomness and incoherence conditions, then the signal $\mathbf{x} = \Psi \boldsymbol{\alpha}$ can be recovered by solving the following convex ℓ_1 optimization problem:

$$\underset{\boldsymbol{\alpha}}{\operatorname{argmin}} \|\boldsymbol{\alpha}\|_1 \quad \text{subject to} \quad \|\Phi \Psi \boldsymbol{\alpha} - \mathbf{y}\|_2 \leq \epsilon, \quad (4)$$

where ϵ is a bound on the noise level. It is worth noting that, in the context of SD reconstructions, the sparsity basis Ψ boils down to the identity matrix,

thus $\mathbf{x} = \boldsymbol{\alpha}$. In (Ramirez-Manzanares et al., 2007; Jian and Vemuri, 2007) the sensing basis Φ , also called *dictionary* in this context, is generated by applying a set of rotations to a given Gaussian kernel (i.e. diffusion tensor) and the sparsest coefficients \mathbf{x} of this linear combination best matching the measurements \mathbf{y} are recovered by solving the following constrained minimization problem:

$$\operatorname{argmin}_{\mathbf{x} \geq 0} \|\mathbf{x}\|_1 \quad \text{subject to} \quad \|\Phi \mathbf{x} - \mathbf{y}\|_2 \leq \epsilon, \quad (5)$$

where the positivity constraint on the FOD values was directly embedded in the formulation of the convex problem. The parameter ϵ can be easily estimated from the data assuming that the samples are contaminated with Gaussian noise, which is normally the case with MRI data with sufficient signal-to-noise ratio (SNR), as shown by Gudbjartsson and Patz (1995). For $\text{SNR} > 2$, in fact, the noise in magnitude MRI images can be assume Gaussian-distributed. Consequently, from a statistical standpoint, the ℓ_2 norm is a suitable choice in the minimization problems to describe the residual noise on the estimate of \mathbf{x} as it identifies with the negative log-likelihood. For simplicity one can also extrapolate the choice of the ℓ_2 norm at lower SNR, independently of statistical considerations.

In this context, however, a statistical estimation of ϵ is not reliable. In fact, since the aim of these reconstruction methods is to reduce the number of measurements, the χ^2 estimator of the noise has a large variance around its mean. This fact is related to the well-known phenomenon of concentration of measure in statistics. To overcome this issue, the reconstruction problem can be re-formulated as a regularized (as opposed to constrained) ℓ_1 minimization as in (Landman et al., 2012; Pu et al., 2011):

$$\operatorname{argmin}_{\mathbf{x} \geq 0} \|\Phi \mathbf{x} - \mathbf{y}\|_2^2 + \beta \|\mathbf{x}\|_1, \quad (6)$$

where the free parameter β controls the trade-off between the data and the sparsity constraints. In general, β depends on the acquisition scheme and the noise level and it must be empirically optimized. Noteworthy, the cost function in (5) and (6) aims at minimizing the ℓ_1 norm of the FOD \mathbf{x} , even though $\sum_i x_i \equiv \|\mathbf{x}\|_1 = 1$ by construction. For this reason, we reckon that these regularized ℓ_1 formulations are intrinsically suboptimal and, in this work, our main goal is to adequately characterize the actual sparsity lying in the FOD.

2.2. Reweighted constrained ℓ_1 minimization

In the aim of adequately characterizing the FOD sparsity, we re-formulate the spherical deconvolution problem as a constrained ℓ_0 minimization problem:

$$\operatorname{argmin}_{\mathbf{x} \geq 0} \|\Phi \mathbf{x} - \mathbf{y}\|_2^2 \quad \text{subject to} \quad \|\mathbf{x}\|_0 \leq k, \quad (7)$$

where $\|\cdot\|_0$ explicitly counts the number of nonzero coefficients and the parameter k represents the expected number of fiber populations in a voxel.

As already stated, the ℓ_0 problems as such are intractable. The reweighting scheme proposed in Candès et al. (2008) proceeds by sequentially solving weighted ℓ_1 problems of the form (7), where the ℓ_0 norm is substituted by a weighted ℓ_1 norm defined as $\|\mathbf{w}\boldsymbol{\alpha}\|_1 = \sum_i \mathbf{w}_i |\alpha_i|$, for positive weights \mathbf{w}_i and where i indexes vector components. At each iteration, the weights are essentially set as the inverse of the values of the solution of the previous problem, i.e. $\mathbf{w}_i^{(t)} \approx 1/\mathbf{x}_i^{(t-1)}$. At convergence, this set of weights makes the weighted ℓ_1 norm independent of the precise value of the nonzero components, thus mimicking the ℓ_0 norm while preserving the tractability of the problem with convex optimization tools. Of course, it is not possible to have infinite weights where the estimated signal values are zero, so that a stability parameter τ must also be added to the signal value in the selection of the weights.

The main steps of the reweighted scheme are reported in the algorithm 1. We empirically set $\tau = 10^{-5}$ and the procedure was stopped if $\frac{\|\mathbf{x}^{(t)} - \mathbf{x}^{(t-1)}\|_1}{\|\mathbf{x}^{(t-1)}\|_1} < 10^{-3}$ between two successive iterations or after 20 iterations. At the first iteration the weighted ℓ_1 norm is the standard ℓ_1 norm given $\mathbf{w} = 1$, and therefore the constraint $\|\mathbf{w}^{(0)}\mathbf{x}\|_1 \leq k$ is a weak bound on the sum of the fiber compartments and does not constitute then a crucial limitation in the procedure. Moreover, the algorithm was found to be quite robust to the choice of k , and differences were not observed for values up to $k = 5$. However, as discussed before, we can expect to have at maximum 2-3 fiber compartments in each voxel and thus in our experiments we fixed $k = 3$. Finally, an explicit constraint $\sum_i \mathbf{x}_i = 1$ might have been added. For the sake of simplicity of the algorithm, in this work this constraint was not included, assuming it is carried over by well-designed bases and the data, as pointed out by Ramirez-Manzanares et al. (2007). In the remaining of the manuscript we will refer to this problem as RSD (Reweighted Sparse Deconvolution).

Algorithm 1 Reweighted ℓ_1 minimization for intra-voxel structure recovery

Input: Diffusion MRI signal $\mathbf{y} \in \mathbb{R}^m$ and sensing basis $\Phi \in \mathbb{R}^{m \times n}$

Output: FOD $\mathbf{x} \in \mathbb{R}^n$

Set the initial status:

$$t \leftarrow 0 \quad \text{and} \quad \mathbf{w}_i^{(0)} \leftarrow 1, \quad i = 1, \dots, n$$

repeat

Solve the problem:

$$\mathbf{x}^{(t)} \leftarrow \underset{\mathbf{x} \geq 0}{\operatorname{argmin}} \|\Phi\mathbf{x} - \mathbf{y}\|_2^2 \quad \text{subject to} \quad \|\mathbf{w}^{(t)}\mathbf{x}\|_1 \leq k$$

Update the weights:

$$\mathbf{w}_i^{(t+1)} = \frac{1}{|\mathbf{x}_i^{(t)}| + \tau}$$

$$t \leftarrow t + 1$$

until stopping criterion is satisfied

$$\mathbf{x} \leftarrow \mathbf{x}^{(t-1)}$$

2.3. Comparison framework

We compared our ℓ_0 -based regularization scheme against other well established state-of-the-art approaches. In particular, we included in the comparison the two regularization schemes (3) and (6), which are based on ℓ_2 and ℓ_1 priors, respectively. In the following, we will refer to these two problems as CSD for the former and L2L1 for the latter. To run CSD reconstructions we made use of the original `mrtrix`¹ implementation, setting the optimal parameters as suggested by the software itself. To solve the L2L1 and RSD problems we used the SParse Modeling Software (SPAMS)², an open-source and very fast optimization toolbox written in C++ for solving various sparse recovery problems. Numerical simulations on synthetic data were performed to *quantitatively assess* the performance of CSD, L2L1 and RSD under controlled conditions. A *qualitative evaluation* of the effectiveness on real human brain data was also carried out.

2.4. Numerical simulations

Independent voxels with two fiber populations crossing at specific angles ($30^\circ - 90^\circ$ range) and with equal volume fractions were synthetically generated. The MRI signal attenuation S corresponding to each voxel configuration was simulated by using the exact expression for particles diffusing in a restricted cylindrical geometry given in (Soderman and Jonsson, 1995). The following parameters were used (Özarslan et al., 2006; Jian and Vemuri, 2007): $L = 5$ mm, $\rho = 5$ μm , $D_0 = 2.02 \times 10^{-3}$ mm^2/s , $\Delta = 20.8$ ms, $\delta = 2.4$ ms. The signal S was contaminated with *Rician noise* (Gudbjartsson and Patz, 1995) as follows:

$$S_{\text{noisy}} = \sqrt{(S + \xi_1)^2 + (\xi_2)^2}, \quad (8)$$

where $\xi_1, \xi_2 \sim \mathcal{N}(0, \sigma^2)$ and $\sigma = S_0/\text{SNR}$ corresponds to a given signal-to-noise ratio. We assumed $S_0 = 1$ without loss of generality.

For each voxel configuration, the signal was simulated at different b-values, $b \in \{500, 1000, \dots, 4000\}$ s/mm^2 , and seven q-space sampling schemes were tested, respectively with 6, 10, 15, 20, 25, 30 and 50 samples equally distributed on half the unit sphere using electrostatic repulsion (Jones et al., 1999) assuming antipodal symmetry in diffusion signal. Six different noise levels were considered, $\text{SNR} = 5, 10, \dots, 30$. For every SNR, 100 repetitions of the same voxel were generated using different realizations of the noise. In our experiments, the actual signal-to-noise ratio in the simulated signal was always in a range where the Gaussian assumption on the noise holds. In the extreme setting with a $\text{SNR} = 5$ on the S_0 and $b = 4000$ s/mm^2 the actual signal-to-noise ratio in the signal was about 1.4.

¹<http://www.brain.org.au/software/mrtrix>

²<http://spams-devel.gforge.inria.fr>

2.5. Evaluation criteria

As the focus of this work is to improve SD reconstructions, we adopted some standard metrics widely used in the literature (Ramirez-Manzanares et al., 2008; Landman et al., 2012; Michailovich et al., 2011) to assess the quality of reconstructions with respect to number and orientation of the fiber populations identified:

- *Probability of false fiber detection.* This metric quantifies the correct assessment of the real number M of populations inside a voxel:

$$P_d = \frac{|M - \tilde{M}|}{M} \cdot 100\%, \quad (9)$$

where \tilde{M} is the estimated number of compartments. As P_d does not distinguish between not recovered fibers and extra compartments found by the reconstruction, we also make use of the following two quantities where needed, n^- and n^+ , explicitly counting the number *under-* and *over-estimated* compartments, respectively.

- *Angular error.* This metric quantifies the angular accuracy in the estimation of the directions of the fiber populations in a voxel:

$$\epsilon_\theta = \frac{180}{\pi} \arccos(\mathbf{d} \cdot \tilde{\mathbf{d}}), \quad (10)$$

where \mathbf{d} is a true direction and $\tilde{\mathbf{d}}$ is its closest estimate. The final value of the metric is an average over all the fiber compartments within a voxel.

Peaks detection was performed using a local maxima search algorithm on the FOD recovered with the three methods. For every direction a neighbourhood of orientations within a cone of 15° was considered and values smaller than 10% of the largest peak were discarded. In the case of CSD, however, we had to increase this threshold to 20% as suggested by Tournier et al. (2007) for removing all the spurious peaks in order to compare with the other two methods.

2.6. Real data

Human brain data was acquired on two young healthy volunteers. Images were collected on a 3T Magnetom Trio system (Siemens, Erlangen, Germany) equipped with a 32-channel head coil using standard DTI protocols routinely used in clinical practice. The two datasets have been acquired at $b = 1000 \text{ s/mm}^2$ using 30 and 20 diffusion gradient directions, respectively, uniformly distributed on half the unit sphere, and in the following they will be referred as `data30` and `data20`. Other acquisition parameters were as follows: TR/TE = 7000/82 ms and spatial resolution = $2.5 \times 2.5 \times 2.5 \text{ mm}$ for dataset `data30`, while TR/TE = 6000/99 ms and spatial resolution = $2.2 \times 2.2 \times 3 \text{ mm}$ for dataset `data20`. The actual SNR in the $b = 0$ images, computed as the ratio of the mean value in a region-of-interest placed in the white matter and the standard deviation of the noise estimated in the background, was about 60 in `data30` and 30 in `data20`.

2.7. Implementation details

In all our experiments, the response function was estimated from the data following the procedure described in Tournier et al. (2004, 2007). In real data, the 300 voxels with the highest fractional anisotropy were selected and a diffusion tensor was fitted from the signal profile in each voxel. In the case of numerical simulations, we generated an additional set of data containing voxels with a single fiber population and applied the same procedure. A different kernel has been estimated for every combination of experimental conditions (b-value, SNR, number of samples).

The same estimated response function was used in all three reconstruction methods considered in this work. This was directly used in the CSD algorithm whereas, in the case of L2L1 and RSD, the dictionary Φ was generated by rotating it along 200 orientations uniformly distributed on half the unit sphere using electrostatic repulsion (Jones et al., 1999). In real data experiments, an additional isotropic compartment was included in Φ to properly model any partial/full contamination with CSF.

Although there are no free parameters to set in CSD and RSD problems (in the latter case we can in fact assume $k = 3$), β has to be empirically estimated in the case of L2L1 reconstructions. We optimised this parameter following the guidelines of Landman et al. (2012), in order to place the method in its best conditions. In numerical simulations, we created an additional training dataset for every combination of experimental conditions (b-value, SNR, number of samples) and 50 reconstructions were performed varying the parameter β from $10^{-4} \beta^*$ to β^* , with $\beta^* = \|\mathbf{2}\Phi^T \mathbf{y}\|_\infty$ computed independently in each voxel. The value providing the best reconstruction (using the above metrics) was then used to run L2L1 on the actual data used for the final comparison. In real data, since the ground-truth is unknown, we set $\beta = 0.1 * \beta^*$ independently in each voxel as suggested in the same work.

3. Results and discussion

We *quantitatively compared* the three reconstruction methods on synthetic data under controlled conditions. In particular, the quality of the reconstructions was evaluated using the metrics introduced above and selectively varying (i) the number of samples and (ii) the b-value of the acquisition scheme, (iii) the noise level and (iv) the crossing angle between the fiber compartments. Results are reported independently for each experimental condition.

Figure 1 reports the performances of the three reconstruction methods as the number of samples changes. We considered seven acquisition schemes from 6 to 50 samples and results are reported for a standard acquisition setup, specifically a shell at $b = 2000 \text{ s/mm}^2$ with a $\text{SNR} = 25$. The quality metrics are reported here as the average value computed over all simulated crossing angles ($30^\circ - 90^\circ$). Looking at plots the effects of reweighting are clear: RSD always outperforms both CSD and L2L1 in identifying the correct number of fiber populations in a voxel (P_d) and results are consistent for all the number of samples

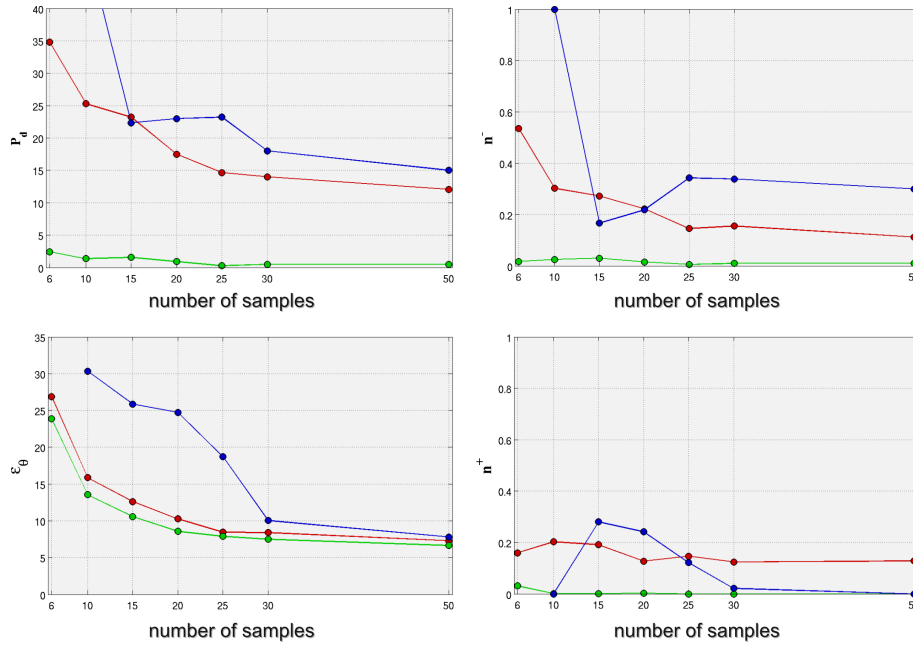


Figure 1: **Quantitative comparison as a function of the number of samples.** The values of the four quality metrics are reported for CSD (blue), L2L1 (red) and RSD (green) as the number of samples changes. The same color-coding is used consistently in all the figures to easily identify each reconstruction method. Values shown here correspond to an experimental setting with $b = 2000$ s/mm² and SNR = 25.

considered. The main benefit of RSD seems to be the drastically decreased number of missed fibers (smaller n^-), even though also the number of over-estimated compartments (n^+) is reduced significantly using RSD as well. Concerning the angular accuracy of the recovered fiber directions (ϵ_θ), reconstructions with RSD always resulted in smaller errors as compared to both CSD and L2L1. For 30 or more samples the difference is not as significant as it is for P_d . For less than 30 samples, however, both L2L1 and RSD show a substantial overall improvement (about 10° to 15°) with respect to CSD, with RSD further improving the accuracy of L2L1 by 1° to 3° on average.

As expected, the accuracy of the reconstructions degraded as the number of samples decreases for all the three methods, although CSD shows a significant degradation with less than 30 samples. This can be explained with the SH representation used internally by CSD. In fact, even though the FOD is a function on the sphere containing high-resolution features by definition, a maximum SH order $l_{max} = 4$ (or less) can be used for acquisitions with less than 30 samples, hence drastically reducing the intrinsic angular resolution of the recovered FOD. At least 30 to 60 samples are normally advised for using CSD, so in our experiments we have actually tested CSD beyond its applicability range. On the

contrary, L2L1 and RSD do not make use of SH and the reconstruction quality degrades more smoothly with the under-sampling rate of the MRI signal. In the following, then, we will focus on two acquisition schemes to further analyze the performances of three methods: (i) in a normal setting with 30 samples and (ii) in a condition of high under-sampling with only 15 samples.

In figure 2 the performances of CSD, L2L1 and RSD are plotted in detail as a function of the crossing angle between the fiber populations. Results are reported for two acquisition schemes using 30 and 15 samples, both simulated at $b = 2000 \text{ s/mm}^2$ and $\text{SNR} = 25$. With 30 samples, no modeling errors occur (as we pointed out before) and the major source of errors for CSD and L2L1 is represented by under-estimation (n^-), with both methods starting to severely miss fibers for crossing angles below $50^\circ/60^\circ$, on the contrary of RSD. In this setting, both CSD and L2L1 tend to recover one single peak lying between the two real fiber compartments and the maximum angular error for the sole estimated compartment is generally upper bounded by half the crossing angle. For this reason the overall performances of CSD and L2L1 do not differ significantly from RSD despite the drastic improvement in terms of P_d , n^- and n^+ . Nonetheless, the ability of reliably recovering fibers also for crossing angles below $50^\circ - 60^\circ$ is very important for fiber-tracking applications which rely on the accurate estimates of white matter orientation, because the propagation of these errors might have dramatic consequences in the final estimated trajectories. In an under-sampling scenario with 15 samples, however, both CSD and L2L1 are less robust and exhibit a higher P_d with a stronger tendency to over-estimate compartments, usually in completely arbitrary directions not even close to the true fiber directions. The overall improvement of RSD on angular accuracy is more evident, with an average enhancement of 1° to 5° with respect to L2L1, while CSD exhibits a severe drop of the performances mainly due to modeling limitations.

Another point worth noting is that CSD achieves slightly better angular accuracy for crossing angles above 60° . The precision of both L2L1 and RSD is in fact affected by the resolution of the grid used to construct the dictionary. In our experiments, 200 directions equally distributed on the sphere were used to build Φ , resulting in a grid resolution of about 10° and thus an intrinsic average error of about 5° . To improve the precision it would be sufficient to increase the number of directions of the discretization which, however, would have serious consequences on the efficiency and stability of the minimization algorithm. Interestingly, recent works of [Tang et al. \(2012\)](#) and [Candes and Fernandez-Granda \(2012\)](#) explored a novel theory of compressed sensing with continuous dictionaries, in the context of which FOD peaks could be thought to be located with infinite precision. This topic will be the subject of future research.

So far CSD, L2L1 and RSD have been compared for given acquisition schemes and a fixed $b = 2000 \text{ s/mm}^2$. Figure 3 reports the quality of the reconstructions with the three approaches as a function of the b-value. The results are shown for 30 and 15 samples with a $\text{SNR} = 25$. CSD tends to miss compartments for low b-values and over-estimate them at higher b (n^+ and n^- are not shown here for brevity). This is even more apparent when decreasing the number of

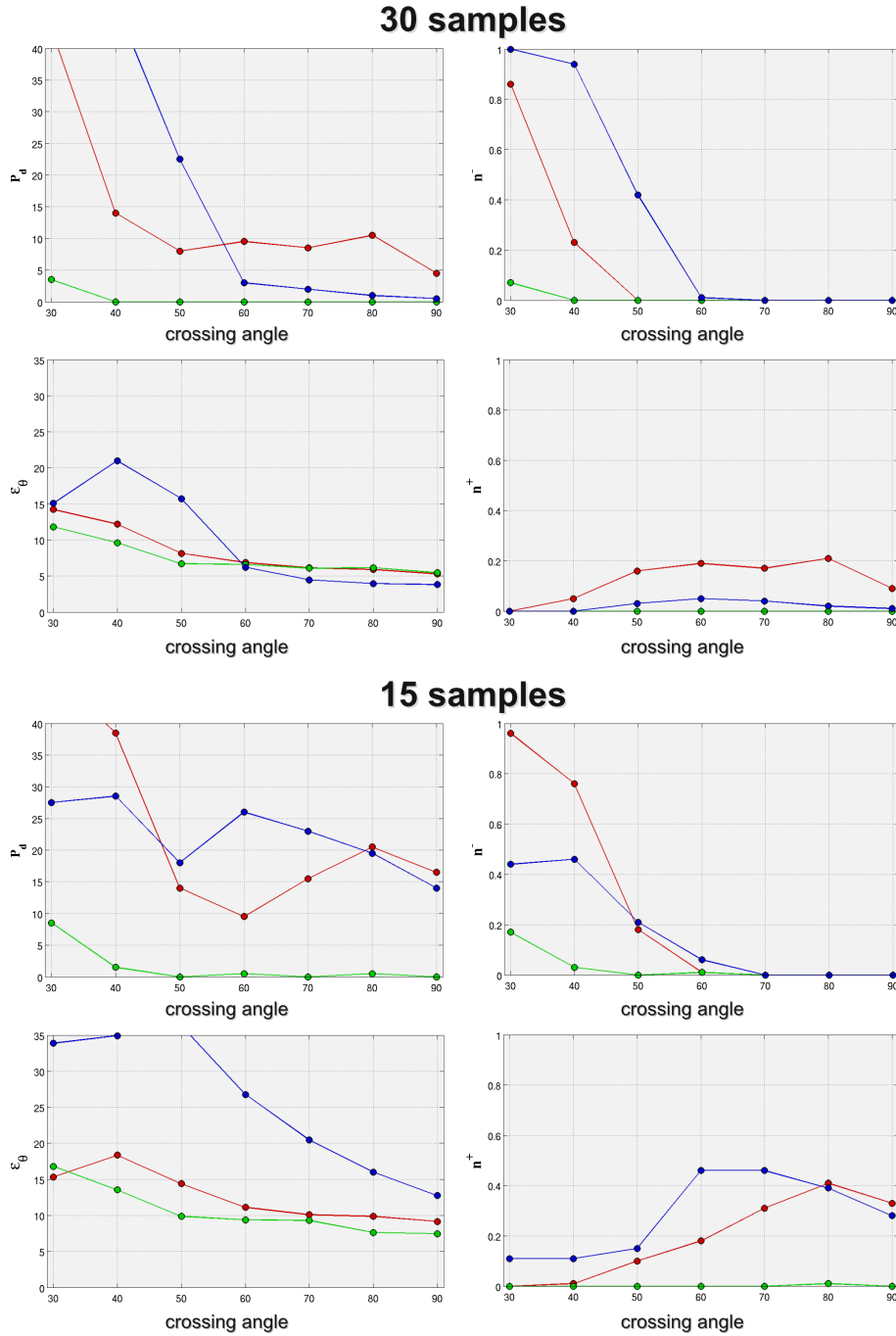


Figure 2: **Quantitative comparison as a function of the crossing angle.** The performances of the three reconstruction methods are detailed separately for each crossing angle used in the simulations. Results are reported for 30 and 15 samples, using the same experimental configuration of Fig. 1, i.e. $b = 2000 \text{ s/mm}^2$ and $\text{SNR} = 25$.

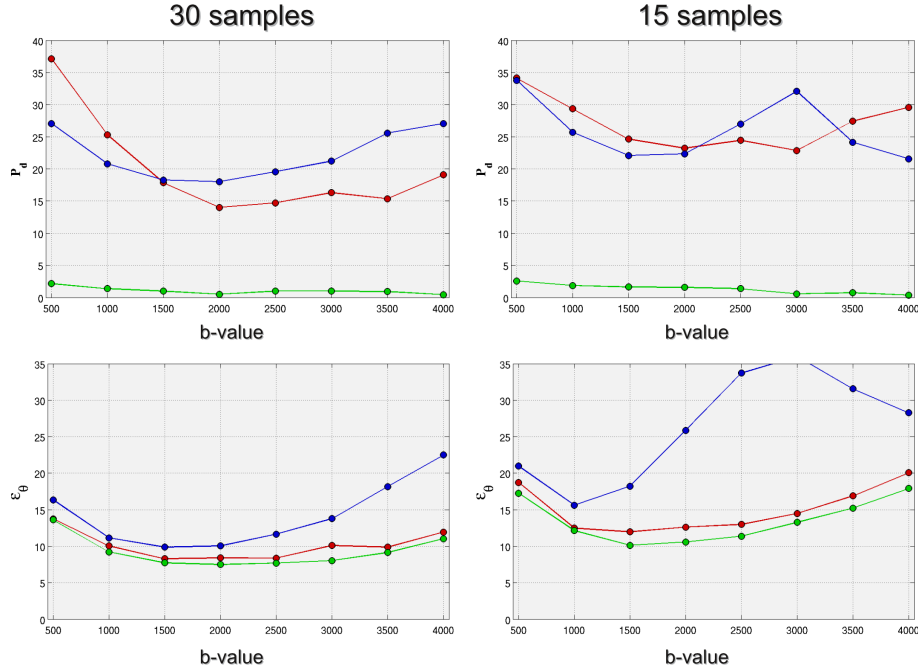


Figure 3: **Quantitative comparison as a function of the b-value.** The dependence of the reconstruction quality on the b-values used in the acquisition is reported here for 30 and 15 samples with a SNR = 25.

samples in the acquisition to 15, where CSD estimates a lot of spurious peaks at high b-values (high n^+) and thus the angular accuracy of the estimated fiber directions drops considerably. Interestingly, L2L1 shows the opposite behavior, under-estimating at high b and over-estimating at low b, although at a smaller rate thus preventing the performances to degrade significantly. Again, in comparison, RSD shows a very stable estimation of the number of fibers.

Concerning the angular accuracy, all methods showed a minimum for ϵ_θ corresponding to $b \approx 1500 - 2500$ s/mm², representing a sort of trade-off between the loss in angular resolution happening at small b-values and the stronger noise influence at higher b. In fact, as in this work we report the noise level as the SNR of the S_0 dataset, images at high b-values will have lower actual SNR, and thus the noise effects will be inherently stronger. Overall, RSD always results in smaller angular errors for the identified fiber compartments than the other two methods. The improvement with respect to L2L1 is moderate (1° to 3° on average), while the difference with CSD is more emphasized as the b-value increases.

Finally, figure 4 compares the robustness to noise of the three reconstruction methods. Six noise levels have been considered, with the SNR of the S_0 dataset varying from 5 to 30. The comparison is reported for 30 and 15 samples at

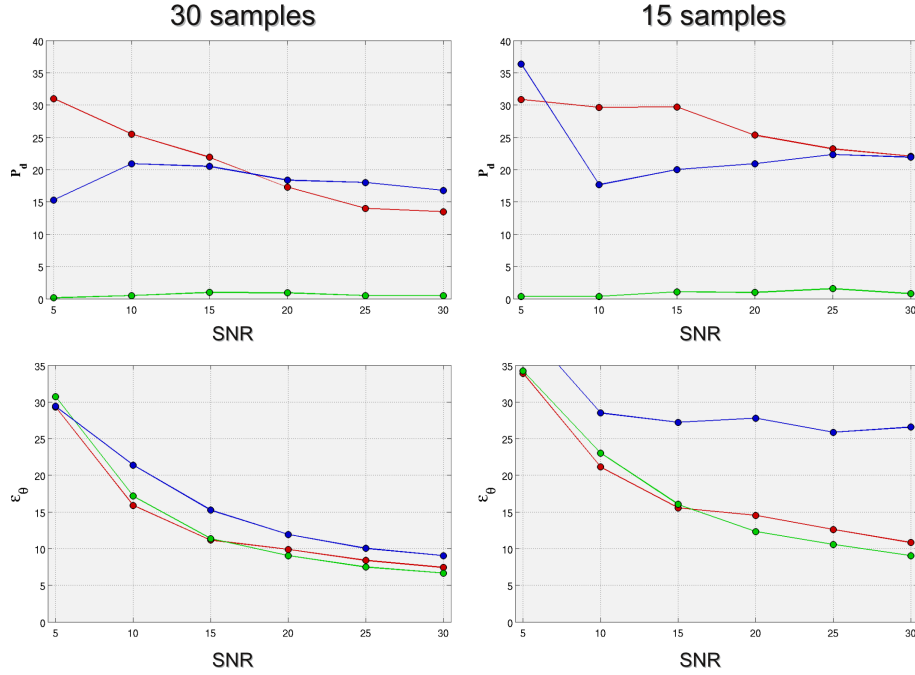


Figure 4: **Quantitative comparison as a function of the SNR.** The robustness to noise of the three reconstruction methods is reported for 30 and 15 samples at $b = 2000 \text{ s/mm}^2$. Reported values for the SNR correspond to the signal-to-noise ratio of the S_0 dataset.

$b = 2000 \text{ s/mm}^2$. The results show that RSD clearly outclasses the other two methods concerning the estimation of the number of compartments (P_d) and results are consistent as the SNR changes. In terms of angular accuracy, ϵ_θ , RSD and L2L1 have very similar ϵ_θ performances, with RSD performing slightly better for $\text{SNR} \geq 15$ and L2L1 for $\text{SNR} \leq 10$. CSD, on the contrary, always provides significantly lower performance (2° to 6° on average) as compared to both RSD and L2L1 at all considered SNRs. The angular accuracy of CSD degrades even more in a high under-sampling regime with 15 samples and it is almost independent of the noise level. This is again consistent with the limitations of the SH representation for acquisitions with very few samples.

The results of the *qualitative evaluation* of the three reconstruction methods in the case of real data are shown in Fig. 5, for both acquisitions with 30 and 20 diffusion gradient directions. Subplots A, B and C correspond to the dataset data_{30} acquired using 30 samples. Even though the acquisition scheme used for this dataset is not the setting where our numerical simulations highlighted the most substantial differences between the three methods, important conclusions can be drawn in favor of RSD. First, the ability of both L2L1 and RSD to properly model the isotropic compartment in voxels with full or partial contamination with CSF is clearly visible. Moreover, comparing B and C we can observe

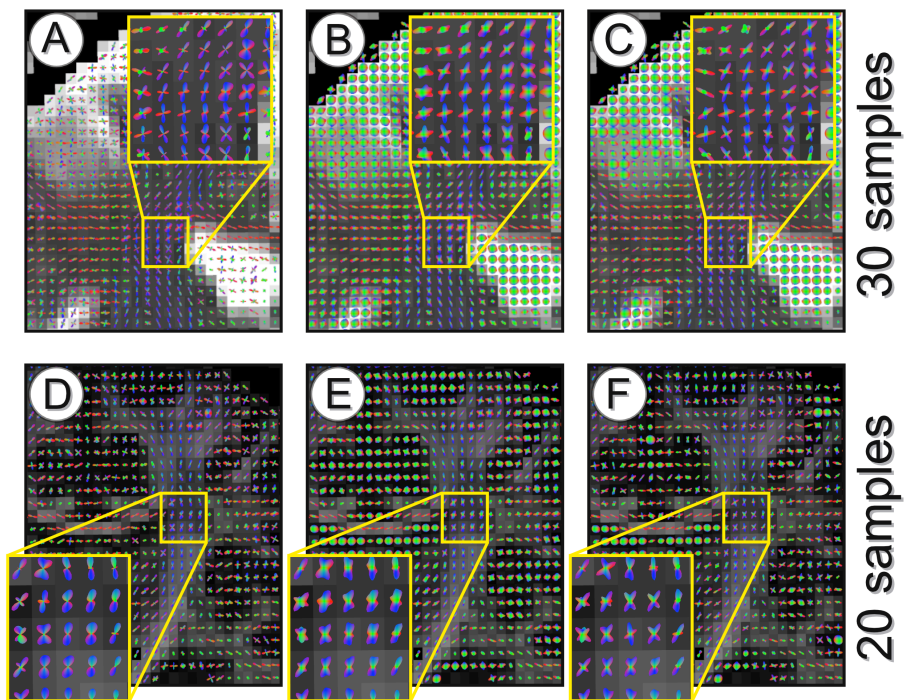


Figure 5: **Qualitative comparison on human brain data.** Reconstructions in the corona radiata region are shown for: CSD (A and D), L2L1 (B and E) and RSD (C and F). Subplots A, B and C correspond to MRI images acquired using 30 samples, while D, E and F are relative to the acquisition with 20 samples. All images have been acquired at $b = 1000$ s/mm².

that RSD successfully differentiates gray matter (light gray regions) from CSF voxels with pure isotropic and fast diffusion (very bright areas), while L2L1 appears unable to distinguish them. The yellow frames in the figures highlight the corona radiata, a well-known region in the white matter containing crossing fibers. As expected from our simulations at this still relatively high number of samples, differences are not obvious between the three methods. However, we observe that RSD clearly results in sharper and more defined profiles than L2L1, whereas the improvements with respect to CSD are confined only to few voxels. The not so good performance of L2L1 might be related to the value chosen for β . In contrast, no free parameter has to be empirically optimized in our approach. When decreasing the acquisition samples to 20 (subplots D, E and F corresponding to `data20` dataset), reconstructions using RSD are definitely much better resolved than both CSD and L2L1. In fact CSD clearly breaks, missing many fiber compartments probably due to the aforementioned representation limitations. The same happens to L2L1, whose reconstructions appear very blurred and noisy.

4. Conclusion

We have proposed to exploit the versatility of compressed sensing and convex optimization to improve spherical deconvolution reconstructions for recovering the white matter intra-voxel configuration with diffusion MRI. We have compared our approach with other well-known state-of-the-art regularization schemes commonly used in this field on both synthetic and real human brain data. Results showed that actually our proposed reweighted constrained ℓ_1 regularization scheme is very effective and indeed improves the reconstructions. This evolution is most remarkable in a high q-space under-sampling regime, thus driving the acquisition cost of HARDI always closer to that of DTI.

Even though we focused here on single voxel experiments, future work will be devoted to study the applicability and the effectiveness of our approach in more sophisticated frameworks exploiting the spatial correlation in the data. Additionally, future research will investigate the use of the recently proposed continuous CS theory with the aim of further improving the accuracy of the reconstructions and reducing the acquisition time.

Acknowledgements

The authors would like to thank Alessandra Griffa for providing the in-vivo MRI data used in this work.

This work was supported in part by the Center for Biomedical Imaging (CIBM) of the Geneva and Lausanne Universities, EPFL, and the Leenaards and Louis-Jeantet foundations, in part by the Swiss National Science Foundation (SNSF) under grant PP00P2-123438, and also by the EPFL-Merck Serono Alliance award.

References

References

- Alexander, D. C., 2005. Maximum entropy spherical deconvolution for diffusion MRI. *Inf Process Med Imaging* 19, 76–87.
- Baraniuk, R., 2007. Compressive Sensing [Lecture Notes]. *IEEE Signal Processing Magazine* 24, 118–121.
- Basser, P., Mattiello, J., Lebihan, D., 1994. MR diffusion tensor spectroscopy and imaging. *Biophysical journal* 66(1), 259–67.
- Candes, E., Fernandez-Granda, C., 03 2012. Towards a mathematical theory of super-resolution. *ArXiv e-prints*.
- Candès, E., Romberg, J., Tao, T., 2006. Robust uncertainty principles: exact signal reconstruction from highly incomplete frequency information. *IEEE Trans. on Information Theory* 52(2), 489–509.
- Candès, E., Wakin, M., Boyd, S., 2008. Enhancing sparsity by reweighted ℓ_1 minimization. *Journal of Fourier Analysis and Applications* 14(5), 877–905.
- Dell’acqua, F., Rizzo, G., Scifo, P., Clarke, R., Scotti, G., Fazio, F., 2007. A model-based deconvolution approach to solve fiber crossing in diffusion-weighted MR imaging. *Biomedical Engineering, IEEE Transactions on* 54 (3), 462–472.
- Donoho, D., 2006. Compressed sensing. *IEEE Trans. on Information Theory* 52(4), 1289–306.
- Gudbjartsson, H., Patz, S., 1995. The Rician distribution of noisy MRI data. *Magn. Reson. Med.* 34(6), 910–4.
- Jeurissen, B., Leemans, A., Jones, D., Tournier, J., Sijbers, J., 2010. Estimating the number of fiber orientations in diffusion MRI voxels : a constrained spherical deconvolution study. In: *ISMRM. Stockholm (Sweden)*, p. 573.
- Jian, B., Vemuri, B. C., Nov 2007. A unified computational framework for deconvolution to reconstruct multiple fibers from diffusion weighted MRI. *IEEE Trans Med Imaging* 26 (11), 1464–1471.
- Jones, D. K., Horsfield, M. A., Simmons, A., Sep 1999. Optimal strategies for measuring diffusion in anisotropic systems by magnetic resonance imaging. *Magn Reson Med* 42 (3), 515–525.
- Landman, B. A., Bogovic, J. A., Wan, H., Elshahaby, F. E. Z., Bazin, P.-L., Prince, J. L., 2012. Resolution of crossing fibers with constrained compressed sensing using diffusion tensor MRI. *Neuroimage* 59(3), 2175–86.

- Mani, M., Jacob, M., Guidon, A., Liu, C., Song, A., Magnotta, V., Zhong, J., may 2012. Acceleration of high angular and spatial resolution diffusion imaging using compressed sensing. In: Biomedical Imaging (ISBI), 2012 9th IEEE International Symposium on. pp. 326–329.
- Merlet, S., Cheng, J., Ghosh, A., Deriche, R., 2011. Spherical Polar Fourier EAP and ODF reconstruction via compressed sensing in diffusion MRI. In: IEEE International Symposium on Biomedical Imaging. pp. 365–371.
- Michailovich, O., Rathi, Y., Dolui, S., 2011. Spatially regularized compressed sensing for high angular resolution diffusion imaging. *IEEE Trans. on Medical Imaging* 30(5), 1100–15.
- Özarslan, E., Shepherd, T., Vemuri, B., Blackband, S., Mareci, T., 2006. Resolution of complex tissue microarchitecture using the diffusion orientation transform (DOT). *NeuroImage* 31 (3), 1086–1103.
- Pu, L., Trouard, T. P., Ryan, L., Huang, C., Altbach, M. I., Bilgin, A., 2011. Model-based compressive diffusion tensor imaging. In: IEEE International Symposium on Biomedical Imaging. pp. 254–257.
- Ramirez-Manzanares, A., Cook, P. A., Gee, J. C., 2008. A comparison of methods for recovering intra-voxel white matter fiber architecture from clinical diffusion imaging scans.
- Ramirez-Manzanares, A., Rivera, M., Vemuri, B., Carney, P., Mareci, T., 2007. Diffusion basis functions decomposition for estimating white matter intravoxel fiber geometry. *IEEE Trans. on Medical Imaging* 26, 1091–102.
- Rathi, Y., Michailovich, O., Setsompop, K., Bouix, S., Shenton, M. E., Westin, C.-F., 2011. Sparse multi-shell diffusion imaging. In: Proceedings of the 14th international conference on Medical image computing and computer-assisted intervention - Volume Part II. MICCAI'11. Springer-Verlag, Berlin, Heidelberg, pp. 58–65.
- Soderman, O., Jonsson, B., 1995. Restricted diffusion in cylindrical geometry. *Journal of Magnetic Resonance, Series A* 117 (1), 94–97.
- Tang, G., Narayan Bhaskar, B., Shah, P., Recht, B., Jul. 2012. Compressed Sensing off the Grid. ArXiv e-prints.
- Tikhonov, A. N., Arsenin, V. Y., 1977. Solutions of ill-posed problems. New York: Winston & Sons.
- Tournier, J.-D., Calamante, F., Connelly, A., 2007. Robust determination of the fibre orientation distribution in diffusion MRI: Non-negativity constrained super-resolved spherical deconvolution. *NeuroImage* 35 (4), 1459–1472.
- Tournier, J.-D., Calamante, F., Gadian, D., Connelly, A., 2004. Direct estimation of the fiber orientation density function from diffusion-weighted MRI data using spherical deconvolution. *NeuroImage* 23 (3), 1176–1185.

- Tristán-Vega, A., Westin, C.-F., 2011. Probabilistic ODF estimation from reduced HARDI data with sparse regularization.
- Wedeen, V., Hagmann, P., Tseng, W.-Y., Reese, T., Weisskoff, R., 2005. Mapping complex tissue architecture with diffusion spectrum magnetic resonance imaging. *Magnetic Resonance in Medicine* 54 (6), 1377–1386.